IEEE Access
Multidisciplinary | Rapid Review | Open Access Journal

Received 24 October 2024, accepted 26 November 2024, date of publication 29 November 2024,
date of current version 9 December 2024.

Digital Object Identifier 10.1109/ACCESS.2024.3508764

RESEARCH ARTICLE

Electric Field Calculation and Comparative Analysis of Conventional and Unconventional Transmission Lines

EASIR ARAFAT, (Graduate Student Member, IEEE), BABAK PORKAR, (Senior Member, IEEE), AND MONA GHASSEMI, (Senior Member, IEEE)

Zero Emission, Realization of Optimized Energy Systems (ZEROES) Laboratory, Department of Electrical and Computer Engineering, The University of Texas at Dallas, Richardson, TX 75080, USA

Corresponding author: Mona Ghassemi (mona.ghassemi@utdallas.edu)

This work was supported in part by the National Science Foundation (NSF) under Award 2306098.

ABSTRACT As global electricity demand continues to rise, innovative transmission line designs are being developed to enhance efficiency and reliability. Recent studies emphasize the urgent need for advanced structures that improve transmission capabilities. In this context, optimally designed unconventional lines with higher natural power emerge as potential game changers. Various electrical, mechanical, and structural aspects must be studied for a new overhead line design. Among them, evaluating these new transmission line designs against established safety standards is crucial, particularly concerning low-frequency (50 or 60 Hz) electric fields generated under these new lines. This paper comprehensively analyzes the electric fields generated by conventional and unconventional overhead transmission lines. By calculating the electric field for each sub-conductor individually, we offer a detailed comparison highlighting the differences in field distribution between these two line types. Our findings indicate that the unconventional transmission lines exhibit a more favorable electric field profile and comply with current exposure limits set by regulatory agencies. This research underscores the potential of unconventional designs to improve safety and minimize environmental impact while addressing the challenges posed by increasing electricity demands.

INDEX TERMS Electric field, overhead line, transmission line, extra high voltage, unconventional lines.

I. INTRODUCTION

The power industry is undergoing rapid expansion to meet the escalating demand for electricity, driven by increasing urbanization, population growth, and technological advancements. Significant progress has been made in generation and distribution systems, notably through the downsizing of electric generators to enhance efficiency, the integration of renewable energy sources like solar and wind, and the deployment of advanced power electronics to facilitate more effective electricity distribution [1], [2]. These innovations are crucial in creating a more resilient and sustainable energy infrastructure. However, the development of transmission lines—a critical component of the energy network—has not kept pace with these advancements. The U.S. high-voltage transmission system, for example, has faced challenges in keeping up with the integration of renewable energy, with the annual construction of new high-voltage lines slowing considerably over the past decade [3]. Additionally, the increasing curtailment of wind and solar energy due to transmission congestion further emphasizes the need for transmission line upgrades [2]. This lag in transmission infrastructure poses a risk to energy reliability and security as demand continues to surge.

To achieve net-zero emissions in the United States by 2050, substantial increases in high-voltage transmission capacity are imperative. Experts estimate that capacity must expand by approximately 60% by 2030 and triple by 2050 to integrate more renewable energy facilities into the grid efficiently [4]. This expansion is vital for accommodating large-scale solar and wind installations, which are increasingly recognized for their role in combating climate change. According to recent

The associate editor coordinating the review of this manuscript and approving it for publication was Zhengmao Li.

studies, a staggering $360 billion will need to be invested in transmission capacity by 2030, with total investments projected to reach around $2.4 trillion by 2050 [5]. This financial commitment reflects the urgency of modernizing our transmission infrastructure to support a sustainable energy future.

The deregulation of the U.S. transmission network has complicated the efficient transfer of power across open markets, resulting in delays in necessary investments in transmission infrastructure. Two primary factors contribute to these delays: first, high-voltage overhead line owners often prioritize profit maximization over infrastructure investment; second, the complexities involved in acquiring right-of-way for new lines pose significant challenges. As the focus on renewable energy sources intensifies—particularly large-scale solar power plants and wind farms—the importance of robust transmission networks becomes even more apparent. These renewable resources are frequently situated far from load centers, necessitating extra-high-voltage (EHV) transmission lines to distribute the generated power efficiently.

A significant hurdle in expanding transmission capacity is the high construction cost associated with new lines. In 2023, building a new 500 kV transmission line in the U.S. was estimated to cost between $3.9 million and $4.8 million per mile [6]. In response to this challenge, researchers explore revolutionary transmission line designs that enhance power transmission density within existing corridors. One promising approach involves rearranging phase configurations and sub-conductors into optimized geometric structures, thereby increasing power delivery capability [7].

Traditional calculations of electric field intensity at ground level are not directly applicable to these unconventional transmission lines. Existing models typically assume symmetrical sub-conductor arrangements within bundle circles; however, this assumption does not hold for unconventional designs, where sub-conductors may be positioned asymmetrically or in varied spatial configurations. To accurately assess the impact of these unconventional designs, reliable methods for calculating electric field intensity are crucial.

Electric field intensity beneath transmission lines is a critical parameter in the electrical design of EHV lines, as it directly impacts human life and the elements of the environment. Various methodologies have been proposed to calculate these fields accurately, ensuring safety and compliance with regulatory standards. For example, some studies have focused on calculating electric fields beneath and on the surfaces of high-voltage conductors, providing insight into the distribution of fields and their potential risks [8], [9], [10], [11]. Other research highlights the importance of field mitigation in areas densely populated with human activities, stressing the necessity of precise electric field control near inhabited regions [12], [13], [14], [15]. Moreover, advanced technologies, such as artificial neural networks (ANNs), have enhanced the accuracy of electric and magnetic field estimations, providing a more efficient alternative to traditional methods [16], [17], [18]. This approach improves predictive accuracy and accelerates field evaluation processes, making it easier to ensure transmission lines comply with safety standards. Additionally, research has demonstrated that the interaction between electric and magnetic fields, especially under simultaneous exposure, can significantly affect the induced electric field in humans, further emphasizing the need for comprehensive safety evaluations [19].

High-intensity electric fields near power transmission lines can adversely affect human health and the environment if they exceed established limits. Guidelines from organizations like the International Commission on Non-Ionizing Radiation Protection (ICNIRP) help set maximum exposure levels for public safety [16], [20]. Field mitigation strategies, such as conductor arrangement adjustments, have significantly reduced electric field intensity under extra-high voltage lines, further highlighting the importance of adhering to these safety limits [15]. Additionally, addressing uncertainties in electric and magnetic field calculations is critical for achieving accurate assessments near overhead lines [20], [21]. Moreover, some optimized models now incorporate various algorithms like genetic algorithms, particle swarm optimization, and differential evolution to improve the precision of field intensity predictions [22].

Studies underscore the importance of refining designing parameters for environmental and operational factors, which were avoided earlier. For example, span configurations and managing conductor sag can significantly influence field distribution, leading to more efficient designs that minimize exposure risks [23]. Some external factors, like bird droppings and pole construction materials, show that they can also alter electric field characteristics near the area and necessitate innovative protective measures to ensure the reliability of transmission systems [24]. In light of this growing body of research, maintaining electric field intensity within acceptable limits is essential when designing new EHV overhead lines [14], [25]. This paper presents a method for calculating electric fields near the right-of-way for unconventional lines, comparing these with conventional designs to highlight the benefits of optimized configurations.

The remainder of this paper is organized as follows. **Section II** provides a detailed explanation of the methodology used for electric field calculation. This includes the theoretical framework, equation derivations, and approaches to analyzing conventional and unconventional transmission lines. **Subsection A** describes the electric field calculation method in detail, while **Subsections B and C** introduce the configurations of the conventional and unconventional overhead transmission lines, respectively. In **Section III**, the results of the electric field calculations are presented and discussed. This section focuses on comparing electric field intensities at various heights and locations near the transmission lines, offering insights into electromagnetic exposure and safety considerations. Finally, **Section IV** summarizes the key findings, addresses the compliance of the designs with established safety guidelines, and suggests future research directions.

II. METHOD OF ELECTRIC FIELD ANALYSIS

A. METHODOLOGY FOR ELECTRIC FIELD CALCULATION

The electric field at a random point in space due to the presence of charge is defined as the electric property associated with that point. In the context of power facilities, which typically operate at low frequencies and involve minimal charge displacement, an electric field is generated around these facilities.

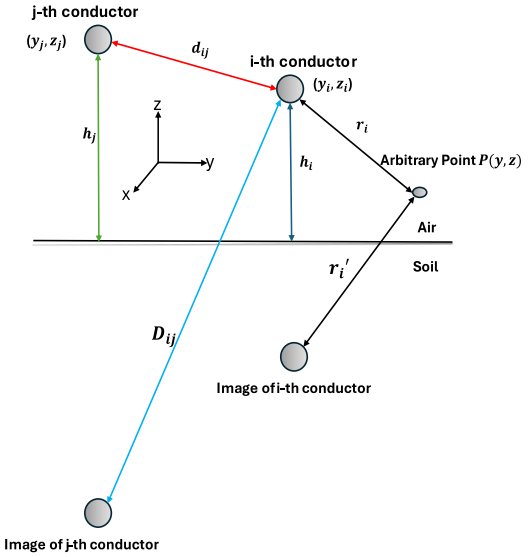

FIGURE 1. The distances between the point charges, their images, and a chosen point.

To calculate the intensity of the electric field at a specific point P (y, z) as illustrated in Fig. 1, in the surroundings of a transmission line, we need to consider two components, one for the horizontal and the other for the vertical:

$$\vec{E} = \left\{\vec{E}_y, \vec{E}_z\right\} \tag{1}$$

For the transmission line, the relationship between charge and voltage is expressed as:

$$[q] = [P]^{-1} . [U] \tag{2}$$

where $[U]$ denotes the voltage phasor matrix relative to the ground, $[q]$ represents the charge matrix, and $[P]$ corresponds to the matrix of Maxwell potential coefficients. These coefficients are determined through two types of elements: mutual and self-elements. For an overhead transmission line with n parallel conductors, these mutual and self-elements are defined by (3) and (4) respectively.

$$P_{ii} = \frac{1}{2\pi\varepsilon_0} \ln \frac{2h_i}{R_i} \tag{3}$$

$$P_{ij} = \frac{1}{2\pi\varepsilon_0} \ln \frac{D_{ij}}{d_{ij}} \tag{4}$$

where ε_0 is the dielectric constant of air, h_i is the vertical coordinate of the i-th conductor, R_i indicates radius of i-th conductor, d_{ij} indicates the shortest distance between the i and j conductors and D_{ij} indicates the shortest distance between i-th conductor and the image of j-th conductors as represented in Fig. 1.

The electric field intensity components at an arbitrary point due to n charges can be computed using (5) and (6).

$$\vec{E}_y(y, z) = \sum_{i=1}^{n} \frac{q_i}{2\pi\varepsilon_0} \left(\frac{y - y_i}{r_i^2} + \Gamma \frac{y - y_i}{r_i'^2} \right) \tag{5}$$

$$\vec{E}_z(y, z) = \sum_{i=1}^{n} \frac{q_i}{2\pi\varepsilon_0} \left(\frac{z - z_i}{r_i^2} + \Gamma \frac{z + z_i}{r_i'^2} \right) \tag{6}$$

In these equations, (y, z) are the coordinates of the point of interest, (y_i, z_i) are the coordinates of the charges, r_i is the shortest distance from the arbitrary point to the i-th point charge, r_i' is the shortest distance between complex images of the i-th point charge and the arbitrary point, as indicated in Fig. 1. The constant Γ denotes the reflection coefficient, which counts the effect of the soil when calculating the electric field at a point. We have considered a value of -1 for this coefficient.

Finally, the total electric field at point P can be expressed as:

$$E_{in} = \sqrt{E_{yn}^2 + E_{zn}^2} \tag{7}$$

B. ANALYSIS OF CONVENTIONAL OVERHEAD TRANSMISSION LINE

This paper analyzes a standard 500 kV transmission line as a benchmark for comparison with our calculated electric field [25]. The layout of its sub-conductors is illustrated in Fig. 2. This particular line features a flat-phase configuration featuring four sub-conductors for each phase, arranged symmetrically in a circular pattern. Each sub-conductor has a diameter of 26.82 mm, and the distance between bundles is 45 cm. The height of the phases is 28 m, and the separation between adjacent phases is 12.3 m. Based on these parameters, the natural power for this design is computed to be 996.0 MW.

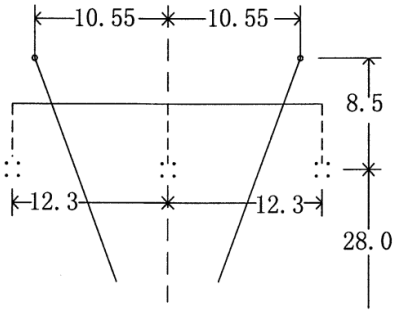

FIGURE 2. Phase and the sub-conductor's configuration of the base case line [25].

As a three-phase system, three alternating voltages (of the same frequency) are carried by three circuit wires and reach their instantaneous peak levels one-third of a cycle apart. As a single circuit 3-phase line, consider the line voltage as $[V]$

which is related to the peak amplitude V_m, initial angle ϕ and the angular frequency ω and presented in (8).

$$[V] = V_m \left[\sin(\omega t+\phi), \sin\left(\omega t+\phi+120^\circ\right), \sin\left(\omega t+\phi+120^\circ\right)\right] \tag{8}$$

Let, J and K are horizontal and vertical coefficients that determine the electric field at a certain point, calculated by (9) and (10). The other parameters of these equations are mentioned in Fig. 1.

$$J_i = (y - y_i)\left(\frac{1}{r_i^2} - \frac{1}{\left(r_i'\right)^2}\right) \tag{9}$$

$$K_i = \left(\frac{(z - z_i)}{r_i^2} - \frac{(z + z_i)}{\left(r_i'\right)^2}\right) \tag{10}$$

Then Eq. (6) will be,

$$\begin{aligned} E_{v1} &= \left(\frac{q_1}{2\pi\epsilon_0}\right) K_1 \\ &= V_m.K_1\left[M_{11}\sin(\omega t+\phi) + M_{12}\sin\left(\omega t+\phi-120^\circ\right)\right. \\ &\quad \left.+M_{13}\sin\left(\omega t+\phi+120^\circ\right)\right] \end{aligned} \tag{11}$$

$$\begin{aligned} E_{v2} &= \left(\frac{q_2}{2\pi\epsilon_0}\right) K_2 \\ &= V_m.K_2\left[M_{21}\sin(\omega t+\phi) + M_{22}\sin\left(\omega t+\phi-120^\circ\right)\right. \\ &\quad \left.+M_{23}\sin\left(\omega t+\phi+120^\circ\right)\right] \end{aligned} \tag{12}$$

$$\begin{aligned} E_{v3} &= \left(\frac{q_3}{2\pi\epsilon_0}\right) K_3 \\ &= V_m.K_3\left[M_{31}\sin(\omega t+\phi) + M_{32}\sin\left(\omega t+\phi-120^\circ\right)\right. \\ &\quad \left.+M_{33}\sin\left(\omega t+\phi+120^\circ\right)\right] \end{aligned} \tag{13}$$

Then, the total vertical component is

$$\begin{aligned} E_{vn} &= V_m\left[(K_1\cdot M_{11}+K_2\cdot M_{21}+K_3\cdot M_{31})\sin(\omega t+\phi)\right. \\ &\quad +(K_1\cdot M_{12}+K_2\cdot M_{22}+K_3\cdot M_{32})\sin\left(\omega t+\phi-120^\circ\right) \\ &\quad \left.+(K_1\cdot M_{13}+K_2\cdot M_{23}+K_3\cdot M_{33})\sin\left(\omega t+\phi+120^\circ\right)\right] \\ &= V_m\left[K_{v1}\sin(\omega t+\phi) + K_{v2}\sin\left(\omega t+\phi-120^\circ\right)\right. \\ &\quad \left.+K_{v3}\sin\left(\omega t+\phi+120^\circ\right)\right] \end{aligned}$$

and in phasor form,

$$E_{vn} = V_m\left[K_{v1}\angle\phi + K_{v2}\angle\left(\phi-120^\circ\right) + K_{v3}\angle\left(\phi+120^\circ\right)\right] \tag{14}$$

Resolving Eq. (14) into real and imaginary parts with $\phi = 0$, we obtain

$$\left.\begin{aligned} \textit{real part} &= K_{v1} - 0.5K_{v2} - 0.5K_{v3} \\ \textit{imaginary part} &= 0 - 0.866K_{v2} + 0.866K_{v3} \end{aligned}\right\} \tag{15}$$

Consequently, the amplitude of the electric field is:

$$\begin{aligned} \hat{E}_{vn} &= \sqrt{\left[(K_{v1}-0.5K_{v2}-0.5K_{v3})^2+0.75\,(K_{v3}-K_{v2})^2\right]}\cdot V_m \\ &= \sqrt{K_{v1}^2+K_{v2}^2+K_{v3}^2-K_{v1}K_{v2}-K_{v2}K_{v3}-K_{v3}K_{v1}}\cdot V_m \\ &= K_v\cdot V_m \end{aligned}$$

The r.m.s. value of the total vertical component at $P(x, y)$ due to all 3 phases will be

$$E_{vn} = \frac{\hat{E}_{vn}}{\sqrt{2}} = K_v\cdot V \tag{16}$$

In a similar manner, the r.m.s. value of a total horizontal component of the field at P due to all 3 phases is

$$\begin{aligned} E_{hn} &= J_h\cdot V \\ &= V.\sqrt{J_{h1}^2+J_{h2}^2+J_{h3}^2-J_{h1}J_{h2}-J_{h2}J_{h3}-J_{h3}J_{h1}} \end{aligned} \tag{17}$$

where,

$$\left.\begin{aligned} J_{h1} &= J_1\cdot M_{11}+J_2\cdot M_{21}+J_3\cdot M_{31} \\ J_{h2} &= J_1\cdot M_{12}+J_2\cdot M_{22}+J_3\cdot M_{32} \\ J_{h3} &= J_1\cdot M_{13}+J_2\cdot M_{23}+J_3\cdot M_{33} \end{aligned}\right\} \tag{18}$$

where the values of J_1, J_2, J_3 are obtained from Eq. (9) for J_i with $i = 1, 2, 3$.

The above equations were coded in MATLAB. For conventional transmission lines, the traditional way is to consider a fictitious conductor instead of a bundle conductor. Then, the above equation gets a slight change. And the change occurs in (3), where R_i (radius of the i-th conductor) becomes a_{eq} (equivalent radius). The radius of the fictitious conductor is determined using (19).

$$a_{eq} = R\left(N.a/R\right)^{1/N} \tag{19}$$

R : bundle radius $= B/\left(2\sin\left(\pi/N\right)\right)$ where B: bundle spacing (spacing between adjacent sub-conductors)

N: number of sub-conductors in a bundle,

a: radius of each sub-conductor

C. ANALYSIS OF UNCONVENTIONAL OVERHEAD TRANSMISSION LINES

We also consider two unconventional 500 kV transmission lines, as referenced in [9]. Unlike conventional lines, these lines employ eight sub-conductors per phase, with their orientation calculated using an optimized algorithm aimed at maximizing natural power (P_n in Eq. (20)) output. The design factors include the phase-to-phase distance, surface electric field, symmetry about the centerline, and ground clearance. The optimization is governed by several key conditions, which can be formulated as follows:

$$\begin{aligned} &\max\{P_n\} \\ &\text{Subject to: a. } D_{i_hj_k} \geq D_{min}\ (i, j \in \{1, 2, 3\}\ and\ i \neq j)\ and \\ &\qquad (h, k \in \{1, 2, \ldots .n\}) \\ &\qquad \text{b. } E_{max} \leq E_{pr} \\ &\qquad \text{c. Symmetry constraint} \\ &\qquad \text{d. } H_{min} \geq H_{pr} \\ &\qquad \text{e. } B_{i,h-k}\ B_{i,h-k} \leq L_{bi-spacer}\, i \in \{1, 2, 3\}\ and \\ &\qquad h, k \in \{1, 2, \ldots .n\} \end{aligned} \tag{20}$$

These constraints guarantee precise adjustment of the subconductor positions. The initial requirement stipulates

that the minimum distance between phases must not be below D_{min}, a value derived from thorough studies on lightning and switching overvoltage within the system. The subsequent condition safeguards the maintenance of surface electric field intensity. The third condition guarantees that sub-conductors exert mechanical loads symmetrically on the tower, while the fourth regulates the ground clearance of the line. Lastly, the fifth condition restricts sub-conductor clearance within a single phase. In this case, phase-to-phase minimum clearance is 6.7 m, the conductor surface electric field is 17.20 kV/cm (rms), and the minimum possible height is 27.775 m. The bi-conductor spacer distance is kept at 2.2 m. The optimization problem mentioned in (8) can be solved using evolutionary search algorithms, but an innovative algorithm is presented to solve it in [26] and [27]. The algorithm is shown in Fig. 3.

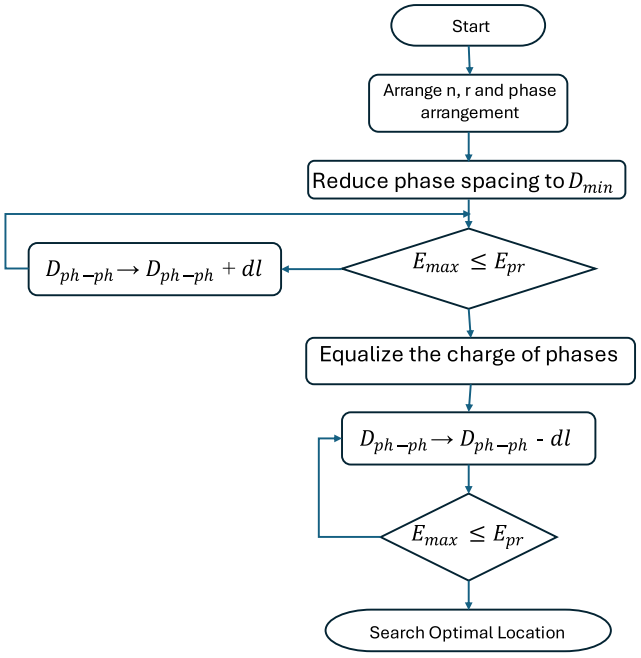

FIGURE 3. Suggested algorithm for determining the optimal locations of sub-conductors.

A horizontal phase configuration is presumed to address the problem utilizing the algorithm. Subsequently, for a specified n and r, The sub-conductors are positioned symmetrically on a circle with a radius r_b, Which is standard for conventional lines. After this, the phase spacing is decreased to D_{min}, as stated in the initial constraint.

Subsequently, the surface electric field is assessed to satisfy the second constraint. If the maximum electric field (E_{max}) is less than or equal to the prescribed value (E_{pr}), the phase spacing is increased until E_{max} equals E_{pr}. Following this, the charges of the phases are equalized to fix the phase positions. Subsequently, employing the direct search algorithm, the positions of the sub-conductors are determined. After obtaining a new set of positions, the natural power is computed. If the combination yields a superior value of P_n and satisfies all five constraints, the location is considered for the second iteration. This iterative process yields numerous solutions. However, only two models are considered for this paper, as depicted below.

In Figs. 4 and 5, we can see the optimal orientations obtained from solving (8) using the algorithm described in Fig. 3. HSIL-1's sub-conductors have a diameter of 20.93 mm. The sub-conductor with the greatest height from the ground is in the outside phases, at 32 m, while the one with the least height is in the central phase, at 24 m.

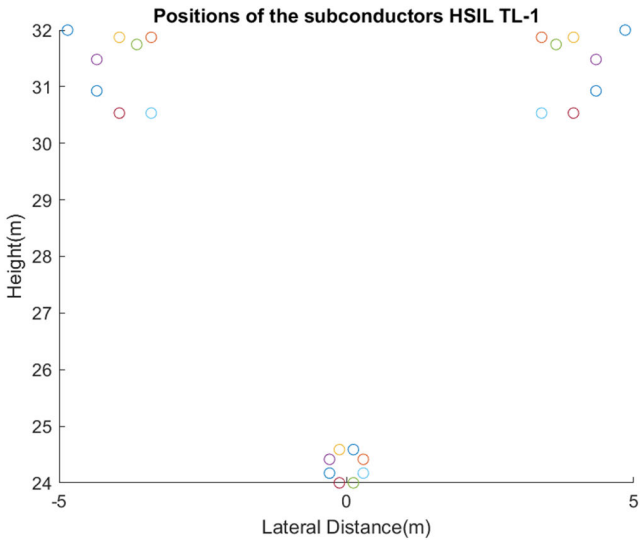

FIGURE 4. Phase and sub-conductor's position of the HSIL-1.

Like HSIL TL1, HSIL TL2 has eight sub-conductors with the same conductor type in each phase. Its width is the same as the conventional line, Fig. 2, 24.6 m. We must consider each sub-conductor separately to calculate the electric field for these two unconventional lines. Because of its orientation, we cannot consider each sub-conductor bundle as one conductor. That's why we must calculate the effect of $8 \times 3 = 24$ conductors with its image conductors. To do this, we used the method discussed previously. The only difference between the conventional and unconventional one is the consideration of radius while determining the potential coefficients. The mutual element of the potential coefficient in (3) considers an actual radius rather than a fictitious radius.

III. RESULTS AND DISCUSSION

The previously outlined method is employed to calculate the electric field distribution for the transmission line (TL) under consideration. This study focuses on two critical measurement points to evaluate the results: one at ground level and another at 1 meter above the ground (especially within the Right of Way (ROW)). The electric field at these two points provides essential insights into the electromagnetic exposure experienced near the transmission line.

Fig. 6 illustrates the intensity of the electric field at ground level. The blue curve in the graph represents the electric field

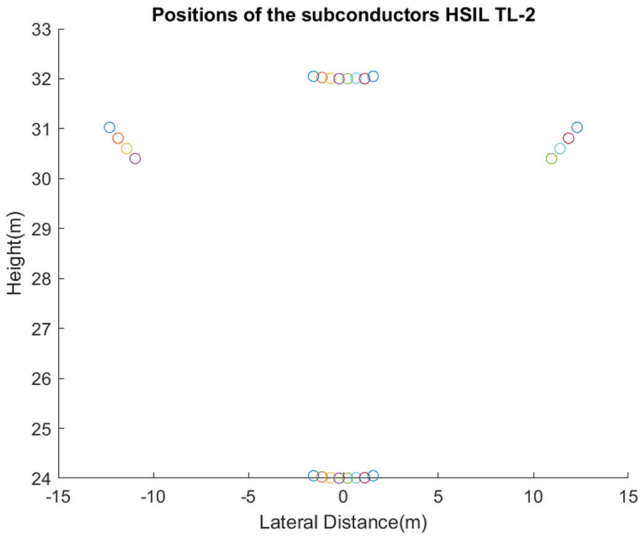

FIGURE 5. Phase and subconductor configuration of the HSIL-2.

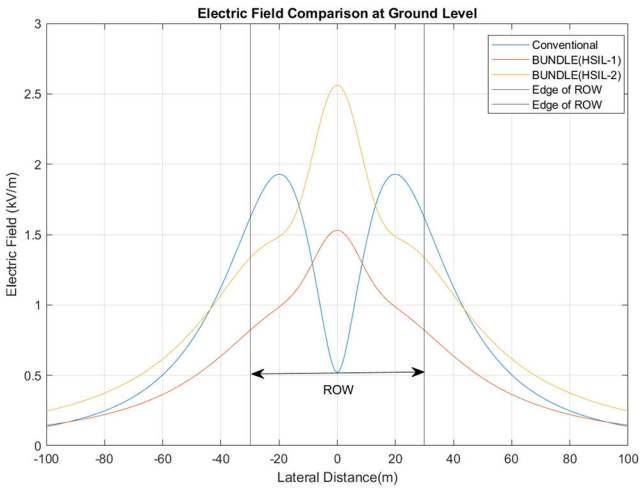

FIGURE 6. Electric field under the high voltage TL at ground level.

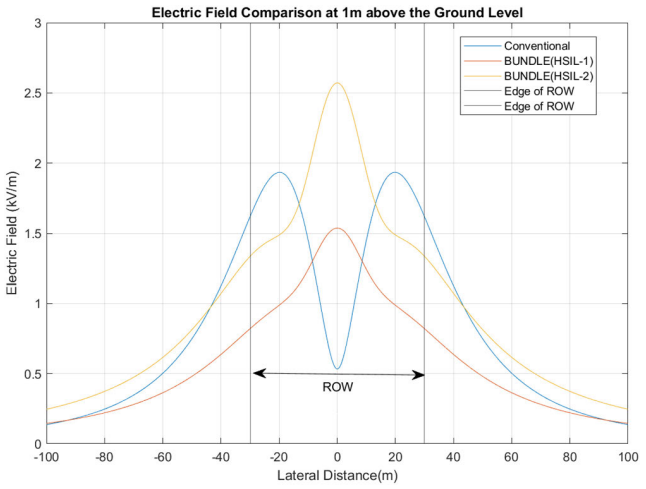

FIGURE 7. Electric Field under the transmission lines at 1 m above the ground.

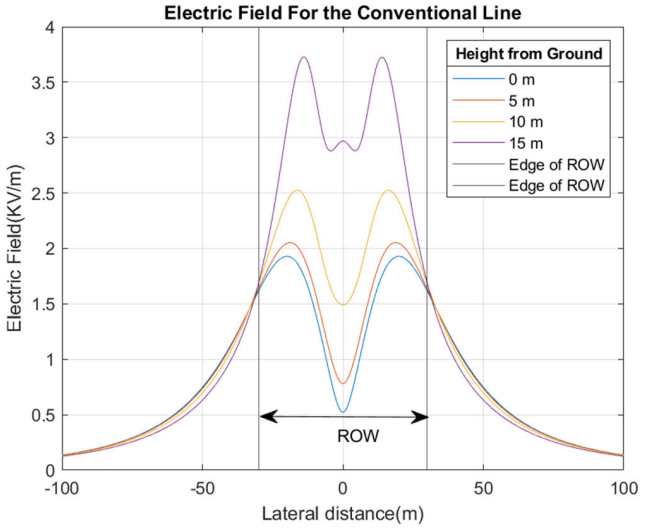

FIGURE 8. Electric Field under the transmission lines at various heights from the ground for the conventional line shown in Fig. 2.

produced by the base case transmission line, which serves as the benchmark for comparison. In contrast, the two proposed unconventional transmission lines exhibit varying electric field behaviors. One of the proposed configurations results in a lower electric field intensity than the base case, indicating a design that minimizes electromagnetic exposure. The other proposed line, while generating a slightly higher electric field than the base case, remains well within the permissible safety limits established for transmission lines in proximity to the right-of-way.

Fig. 7 shows another plot of the electric field above the ground. Like the previous graph, this graph shows that the electric field is under the acceptable limit, even 1 m above the ground.

We need to consider different levels to better understand the electric field distribution of the lines. Figs. 8, 9, and 10 will give us a better view of the electric field distributions. These figures show that the electric fields become more skewed as they rise from the ground, especially for the unconventional transmission lines.

Though the electric fields for the unconventional lines are skewed and raised higher than those for the conventional line, their amounts are still under the acceptable limits, discussed in Tables 1 and 2, at the edge of ROW, even at a height of 15 m from the ground.

The figures presented clearly show that the electric field at the edge of the right-of-way is comparable to that of a conventional line. In this regard, our primary focus should be on its acceptance. The ICNIRP reports from 1998 and 2010, which provide guidelines on exposure limits, are referenced below [28], [29].

Exposure limits can exhibit significant variations across the spectrum, ranging from extremely low frequencies to radio frequencies. Even within the range of extremely

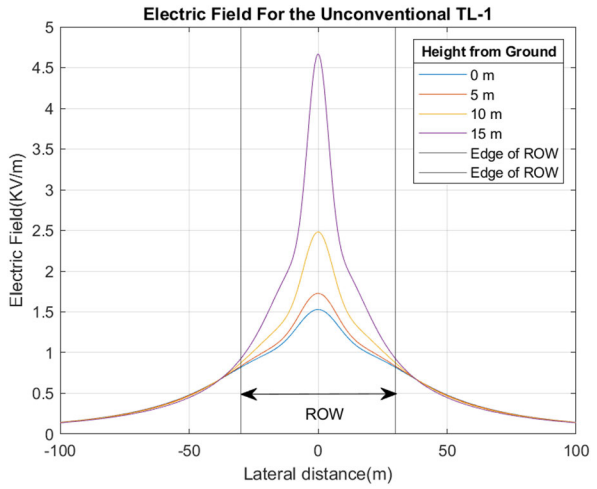

FIGURE 9. Electric field under the transmission lines at various heights for the unconventional TL-1.

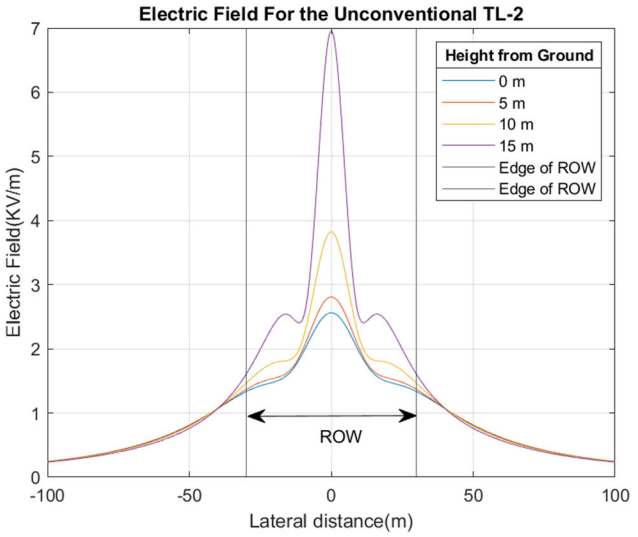

FIGURE 10. Electric field under the transmission lines at various heights for the unconventional TL-2.

low frequencies pertinent to power systems, distinctions between 50 Hz and 60 Hz frequencies can arise.

ICNIRP, an international commission for non-ionizing radiation protection, states that its guidelines are based solely on scientific evidence. Governments may consider additional factors when deciding whether and how to adopt these guidelines. The 1998 ICNIRP guidelines for power frequencies' occupational exposure set the fundamental restriction at 10 mA/m^2. For the public, there is an additional safety factor of 5, resulting in an essential limitation of 2 mA/m^2. It's important to note that these restrictions apply specifically to the central nervous system and not the whole body. Concerning reference levels, the 1998 ICNIRP guidelines set them at 500 μT and 10 kV/m for workers and 100 μT and 5 kV/m for the public at 50 Hz. In contrast, the 2010 ICNIRP guidelines set reference levels at 1000 μT and 10 kV/m for workers and 200 μT and 5 kV/m for the public at 50 Hz. In 1999, the European Union also put forth a public exposure recommendation that included values directly from the ICNIRP 1998 guidelines. No federal exposure limits have been established for extremely low frequency (ELF) electromagnetic fields (EMFs) in the United States. However, six states have implemented exposure limits, primarily focusing on regulations concerning power lines [30].

The values in Tables 1 and 2 compare well, revealing that the electric field at the right-of-way edge of our proposed

TABLE 1. The 1998 and 2010 ICNRP guidelines on exposure limits.

The 1998 ICNIRP Guidelines

	50 Hz	60 Hz	units
Occupational			
Basic Restriction	10	10	mA/m^2
Magnetic Field reference level	500	417	µT
Electric Field reference level	10	8.33	kV/m
General Public			
Basic Restriction	2	2	mA/m^2
Magnetic Field reference level	100	83	µT
Electric Field reference level	5	4.167	kV/m

The 2010 ICNIRP Guidelines

	50 Hz	60 Hz	units
Occupational			
Basic Restriction: Head	100	120	mV/m
Basic Restriction: whole body	800	800	mV/m
Magnetic Field reference level	1000	1000	µT
Electric Field reference level	10	8.33	kV/m
General Public			
Basic Restriction: Head	20	24	mV/m
Basic Restriction: whole body	400	400	mV/m
Magnetic Field reference level	200	200	µT
Electric Field reference level	5	4.167	kV/m

TABLE 2. The EMF exposure limits for overhead lines in six US states.

State	Area Where Limits Apply		Field	Limit
Florida	Edge of Right of Way		Electric	2 kV/m
		230 kV lines	Magnetic	15 µT
		500 kV lines		20 µT
	Anywhere	69-230 kV lines	Electric	8 kV/m
		500 kV lines		10 kV/m
Minnesota	Anywhere		Electric	8 kV/m
Montana	Edge of ROW	Maybe waived by the landowner	Electric	1 kV/m
	Road Crossings		Electric	7 kV/m
New Jersey	Edge of Right of Way		Electric	3 kV/m
New York	Edge of Right of Way		Electric	1.6 kV/m
			Magnetic	20 µT
	Public Road Crossings		Electric	7 kV/m
	Private Road Crossings		Electric	11 kV/m
	Anywhere		Electric	11.8 kV/m
Oregon	Accessible or inhabited areas		Electric	9 kV/m

lines remains well below the threshold established by various organizations.

IV. CONCLUSION

This paper presents a comparative study of the electric fields generated by two unconventional transmission line designs and a conventional 500 kV transmission line, aiming to assess whether the proposed designs comply with internationally established exposure limits. By employing a rigorous analytical method, we computed the electric field intensities at ground level and 1 meter above the ground, focusing on electromagnetic exposure at various critical points around the transmission lines.

The results demonstrate that, while the unconventional designs exhibit variations in electric field intensity compared to the conventional design, both proposed configurations remain well within the permissible safety limits. Specifically, one of the unconventional lines generates a lower electric field than the base case, and the other produces a slightly higher field intensity. However, both remain compliant with international standards, including those outlined by the International Commission on Non-Ionizing Radiation Protection (ICNIRP) for public exposure.

Further analysis at different heights above ground (up to 15 meters) revealed a skewed distribution of the electric field for the unconventional transmission lines. Nonetheless, these variations still adhere to the acceptable thresholds at the edge of the right-of-way, ensuring safe electromagnetic exposure levels across different heights and distances from the lines. Moreover, besides the higher natural power of the unconventional designs, they meet exposure guidelines set by both the ICNIRP and regulatory bodies from various regions, including the European Union and certain U.S. states.

Overall, this study confirms that the innovative subconductor configurations used in unconventional transmission lines provide a viable solution for enhancing transmission capacity while maintaining compliance with strict electromagnetic exposure limits. These results support the feasibility of adopting unconventional designs for future high-capacity transmission projects, balancing efficiency with safety considerations.

REFERENCES

[1] B. Dhamala and M. Ghassemi, "Comparative study of transmission expansion planning with conventional and unconventional high surge impedance loading (HSIL) lines," in *Proc. IEEE Power Energy Soc. Gen. Meeting (PESGM)*, Jul. 2024, pp. 1–5.

[2] B. Dhamala and M. Ghassemi, "An extra-high voltage test system for transmission expansion planning studies considering single contingency conditions," *Electronics*, vol. 13, no. 19, p. 3937, Oct. 2024.

[3] B. Dhamala and M. Ghassemi, "A test system for transmission expansion planning studies," *Electronics*, vol. 13, no. 3, p. 664, Feb. 2024.

[4] B. Dhamala and M. Ghassemi, "Smart transmission expansion planning based on the system requirements: A comparative study with unconventional lines," *Energies*, vol. 17, no. 8, p. 1912, Apr. 2024.

[5] E. Larson, "Net-zero America: Potential pathways, infrastructure, and impacts," interim report, Princeton University, Princeton, NJ, 2020.

[6] *MISO (Midcontinent Independent System Operator)*, document MTEP23, 2023.

[7] M. Ghassemi, "High surge impedance loading (HSIL) lines: A review identifying opportunities, challenges, and future research needs," *IEEE Trans. Power Del.*, vol. 34, no. 5, pp. 1909–1924, Oct. 2019.

[8] M. M. Samy, R. M. Radwan, and S. Akef, "Calculation of electric fields underneath and on conductor surfaces of ultra high voltage transmission lines," in *Proc. IEEE Int. Conf. Environ. Electr. Eng. IEEE Ind. Commercial Power Syst. Eur.*, Jun. 2017, pp. 1–8.

[9] E. Arafat, B. Porkar, and M. Ghassemi, "Electric field comparison of conventional transmission line with unconventional transmission line," in *Proc. IEEE Texas Power Energy Conf. (TPEC)*, Feb. 2024, pp. 1–5.

[10] R. M. Radwan, A. M. Mahdy, M. Abdel-Salam, and M. M. Samy, "Electric field mitigation under extra high voltage power lines," *IEEE Trans. Dielectr. Electr. Insul.*, vol. 20, no. 1, pp. 54–62, Feb. 2013.

[11] M. Z. D. León and P. S. G. S. M, "Development of an efficient method to calculate the electric field produced by power transmission lines considering the buckling of their conductors and the change of trayectory of the lines," in *Proc. IEEE Colombian Caribbean Conf. (C3)*, Nov. 2023, pp. 1–5.

[12] M. H. Elmashtoly, O. E. Gouda, M. Lehtonen, and M. M. F. Darwish, "Mitigation of the electric field under EHVTL in limited space crowded with human activities," *IEEE Access*, vol. 12, pp. 41009–41018, 2024.

[13] M. Bonato, E. Chiaramello, M. Parazzini, P. Gajsek, and P. Ravazzani, "Extremely low frequency electric and magnetic fields exposure: Survey of recent findings," *IEEE J. Electromagn., RF Microw. Med. Biol.*, vol. 7, no. 3, pp. 1–13, Sep. 2023.

[14] T. N. Tefera, G. S. Punekar, K. Ibrahim Yassin, and M. Berhanu Tuka, "Comparative analysis of 500 kV double-circuit transmission line electric field intensity: Ethiopian lines compliance with ICNIRP," *IEEE Access*, vol. 12, pp. 76359–76366, 2024.

[15] A. Z. E. Dein, O. E. Gouda, M. Lehtonen, and M. M. F. Darwish, "Mitigation of the electric and magnetic fields of 500-kV overhead transmission lines," *IEEE Access*, vol. 10, pp. 33900–33908, 2022.

[16] A. Alihodzic, A. Mujezinovic, and E. Turajlic, "Electric and magnetic field estimation under overhead transmission lines using artificial neural networks," *IEEE Access*, vol. 9, pp. 105876–105891, 2021.

[17] S. Alipour Bonab, W. Song, and M. Yazdani-Asrami, "A new intelligent estimation method based on the cascade-forward neural network for the electric and magnetic fields in the vicinity of the high voltage overhead transmission lines," *Appl. Sci.*, vol. 13, no. 20, p. 11180, Oct. 2023.

[18] E. Turajlic, A. Alihodzic, and A. Mujezinovic, "Artificial neural network models for estimation of electric field intensity and magnetic flux density in the proximity of overhead transmission line," *Radiat. Protection Dosimetry*, vol. 199, no. 2, pp. 107–115, Feb. 2023.

[19] Y. Sekiba, S. Kodera, K. Yamazaki, and A. Hirata, "Calculation of electric field induced in the human body for simultaneous exposure to spatially uniform ELF electric and magnetic fields with a phase difference," *IEEE Access*, vol. 11, pp. 95455–95466, 2023.

[20] Y. Zhang, G. Zhang, Z. Feng, N. Li, J. Liu, L. Ding, and X. Wu, "Design and application of a power frequency electric field measuring device for a high-humidity environment," *IET Sci., Meas. Technol.*, vol. 18, no. 6, pp. 289–299, Apr. 2024.

[21] A. Alihodzic, A. Mujezinovic, E. Turajlic, and M. M. Dedovic, "Determination of electric and magnetic field calculation uncertainty in the vicinity of overhead transmission lines," *J. Microw., Optoelectronics Electromagn. Appl.*, vol. 21, no. 3, pp. 392–413, Sep. 2022.

[22] D. Rabah, C. Abdelghani, and H. Abdelchafik, "Efficiency of some optimisation approaches with the charge simulation method for calculating the electric field under extra high voltage power lines," *IET Gener., Transmiss. Distrib.*, vol. 11, no. 17, pp. 4167–4174, Nov. 2017.

[23] A. Z. El Dein, M. A. A. Wahab, M. M. Hamada, and T. H. Emmary, "The effects of the span configurations and conductor sag on the electric-field distribution under overhead transmission lines," *IEEE Trans. Power Del.*, vol. 25, no. 4, pp. 2891–2902, Oct. 2010.

[24] W. Wang, Z. Ma, Y. Fan, J. Ma, K. Liu, Y. Wang, and H. Xu, "Analysis and protection studies of bird droppings falling on the electric field distribution near the 330-kV transmission line V-Type composite insulators," *IEEE Access*, vol. 12, pp. 97938–97950, 2024.

[25] H. Wei-Gang, "Study on conductor configuration of 500-kV chang-fang compact line," *IEEE Trans. Power Del.*, vol. 18, no. 3, pp. 1002–1008, Jul. 2003.

[26] M. A. Khan and M. Ghassemi, "A new unusual bundle and phase arrangement for transmission line to achieve higher natural power," in *Proc. North Amer. Power Symp. (NAPS)*, Oct. 2023, pp. 1–5.

[27] M. A. Khan and M. Ghassemi, "A new method for calculating electric field intensity on subconductors in unconventional high voltage, high power density transmission lines," in *Proc. IEEE Conf. Electr. Insul. Dielectric Phenomena (CEIDP)*, Oct. 2023, pp. 1–4.
[28] A. Ahlbom, E. Cardis, A. Green, M. Linet, D. Savitz, and A. Swerdlow, "Review of the epidemiologic literature on EMF and health," *Environ. Health Perspect.*, vol. 109, p. 911, Dec. 2001.
[29] *ICNIRP Guidelines for 50/60 Hz Exposure Limits*. Accessed: Sep. 20, 2024. [Online]. Available: http://www.emfs.info/limits/5060-2/
[30] (2021). *BOLD, Transmission's Future Today; High Capacity, High Efficiency, Low Profile*. Accessed: Oct. 15, 2024. [Online]. Available: https://usea.org/sites/default/files/event-/AEPBoldTransmission Description11.13.2015.pdf

EASIR ARAFAT (Graduate Student Member, IEEE) received the B.S. degree from Bangladesh University of Engineering and Technology (BUET), Bangladesh. He is currently pursuing the Ph.D. degree in electrical engineering with The University of Texas at Dallas, Richardson, TX, USA. His research interests include power systems design and grid stability using optimization and machine learning.

BABAK PORKAR (Senior Member, IEEE) received the B.Sc. degree from the Sharif University of Technology, in 1999, the M.Sc. degree from Iran University Science of Technology, in 2002, and the Ph.D. degree (Hons.) from the Sharif University of Technology, in 2008, all in electric power engineering. He was a Technical Consultant for several companies and utilities. He is currently with The University of Texas at Dallas, Richardson, TX, USA.

MONA GHASSEMI (Senior Member, IEEE) is currently an Associate Professor and the Chairholder of Texas Instruments Early Career Award, Department of Electrical and Computer Engineering, The University of Texas at Dallas. She has authored over 200 peer-reviewed journal and conference papers and three book chapters. Her research interests include electrical insulation materials and systems, high voltage/field engineering and technology, power systems, and plasma science. She was a member of the Nominations and Appointments Committee of the IEEE Dielectrics and Electrical Insulation Society (DEIS) and the At-Large Member of the Administrative Committee of the IEEE DEIS. She is the Vice-President (Technical) of IEEE DEIS, a DEIS Representative of the IEEE USA Public Policy Committee on Transportation and Aerospace Policy (CTAP) and USA Technology Policy Council Research and Development Policy Committee, a DEIS Technical Committee Member on Dielectrics and Electrical Insulation for Transportation Electrification, and a member of the Education Committee of IEEE DEIS. She received the three most prestigious and most competitive career awards: the Department of Energy Early Career Research Program Award, the National Science Foundation CAREER Award, and the Air Force Office of Scientific Research Young Investigator Research Program Award. She received the 2020 Contribution Award from *IET High Voltage* and four best paper awards. She is an Associate Editor of IEEE TRANSACTIONS ON DIELECTRICS AND ELECTRICAL INSULATION, IEEE TRANSACTIONS ON INDUSTRY APPLICATIONS, *IET High Voltage*, *International Journal of Electrical Engineering Education*, and *Power Electronic Devices and Components*; the Guest Editor of *Aerospace* and *Energies*; and an Associate Guest Editor of IEEE JOURNAL OF EMERGING AND SELECTED TOPICS IN POWER ELECTRONICS.